Photocontrolled DNA binding of a receptor-targeted organometallic ruthenium(II) complex

Flavia Barragán,[ab] Paula López-Senín,[a] Luca Salassa,[c] Soledad Betanzos-Lara,[c] Abraha Habtemariam,[c] Virtudes Moreno,[b] Peter J. Sadler*[c] and Vicente Marchán*[a]

[a]*Departament de Química Orgànica and IBUB, Universitat de Barcelona, Barcelona, E-08028, Spain.* [b]*Departament de Química Inorgànica, Universitat de Barcelona, Barcelona, E-08028, Spain.* [c]*Department of Chemistry, University of Warwick, Coventry, CV4 7AL, UK. E-mail: P.J.Sadler@warwick.ac.uk (PS), vmarchan@ub.edu (VM).*

Supporting Information Placeholder

ABSTRACT: A photoactivated ruthenium(II) arene complex has been conjugated to two receptor-binding peptides, a dicarba analogue of octreotide and the RGD tripeptide. These peptides can act as "tumor targeting devices" since their receptors are overexpressed on the membranes of tumor cells. Both ruthenium-peptide conjugates are stable in aqueous solution in the dark, but upon irradiation with visible light, the pyridyl-derivatized peptides were selectively photodissociated from the ruthenium complex, as inferred by UV-vis and NMR spectroscopy. Importantly, the reactive aqua species generated from the conjugates, $[(\eta^6\text{-}p\text{-cym})Ru(bpm)(H_2O)]^{2+}$, reacted with the model DNA nucleobase 9-ethylguanine, as well as with guanines of two DNA sequences, $^{5'}$dCATGGCT and $^{5'}$dAGCCATG. Interestingly, when irradiation was performed in the presence of the oligonucleotides, a new ruthenium adduct involving both guanines was formed as a consequence of the photo-driven loss of *p*-cymene from the two monofunctional adducts. The release of the arene ligand and the formation of a ruthenated product with a multidentate binding mode might have important implications for the biological activity of such photoactivated ruthenium(II) arene complexes. Finally, photoreactions with the peptide-oligonucleotide hybrid, Phac-His-Gly-Met-linker-p$^{5'}$dCATGGCT, also led to arene release and to guanine adducts including a GG chelate. The lack of interaction with the peptide fragment confirms the preference of such organometallic ruthenium(II) complexes for guanine over other potential biological ligands such as histidine or methionine amino acids.

Introduction. Cisplatin and its second-generation derivatives (carboplatin and oxaliplatin) are successful drugs for the treatment of some types of cancer.[1] However their use is sometimes accompanied by severe toxic side-effects together with the development of resistance in cells, and their limited spectrum of activity. This has stimulated the search for other innovative metal-based anticancer drugs. The main challenge concerns the improvement of targeting strategies either by designing transition metal complexes with ligands that might improve cellular uptake and tumor selectivity, or by using non-toxic pro-drugs whose activity might be triggered within cancer cells.[2] There are several examples of metal complexes that have been conjugated to carrier molecules such as folate, delivery peptides or nanoparticles.[3] Although the covalent attachment to a biological vector is expected to have a positive effect on the delivery of the metal-based drug to cancer cells, it must also be borne in mind that the carrier molecule might affect activity, especially in those cases where the final target is a biomacromolecule (e.g. DNA, RNA or proteins).

Photochemical activation of a metal anticancer pro-drug is a promising strategy since its activity can be triggered by irradiation directly within the tumor.[4] Spatial and temporal control over release of the active species should result in greater selectivity and, consequently, in a reduction of side-effects since the cytotoxicity of the anticancer agent will be limited to the irradiated area. For example, octahedral diazido platinum(IV) compounds are potently cytotoxic towards cancer cells only when irradiated with light and can form Pt-nucleotide DNA cross-links.[5]

In the case of organometallic complexes, we have recently described a pseudooctahedral piano-stool Ru(II) arene complex, $[(\eta^6\text{-}p\text{-cym})Ru(bpm)(py)]^{2+}$, that can also be activated by visible light.[6] Aqueous solutions of the complex are stable in the dark but photodissociation of the Ru-pyridine bond occurs under irradiation with visible light, so providing a mechanism for activation.[7] In addition, the ability of the reactive aquated species to bind to 9-ethylguanine suggests a potential route to bind to biomolecules such as DNA nucleobases. Since the cytotoxicity of some organometallic Ru(II) complexes has been correlated with DNA binding, $[(\eta^6\text{-}p\text{-cym})Ru(bpm)(py)]^{2+}$ represents a candidate in the search for new photoactive metal-based anticancer drugs.[8] Here we propose a strategy for improving selectivity against cancer cells based on the covalent attachment of a delivery peptide to the ruthenium(II) complex through the pyridine ligand. As shown in Scheme 1, photolysis with visible light could initiate ligand dissociation and, consequently, the separation of both entities with the concomitant generation of the activated aqua species **1**. It is expected that the peptide fragment will improve the aqueous solubility and the cellular uptake of the ruthenium-based drug whilst maintaining its mechanism of action, via light-induced ligand release and subsequent interaction with biomolecules such as DNA. This strategy would generate ruthenium-based pro-drugs with a double mechanism of selectivity: the specificity brought by the delivery peptide and the photochemical activation of the ruthenium complex which will would provide control of the fundamental step in the mechanism of action of such Ru(II) compounds.

Scheme 1. Structure of the conjugates synthesized and schematic representation of the photodissociation process

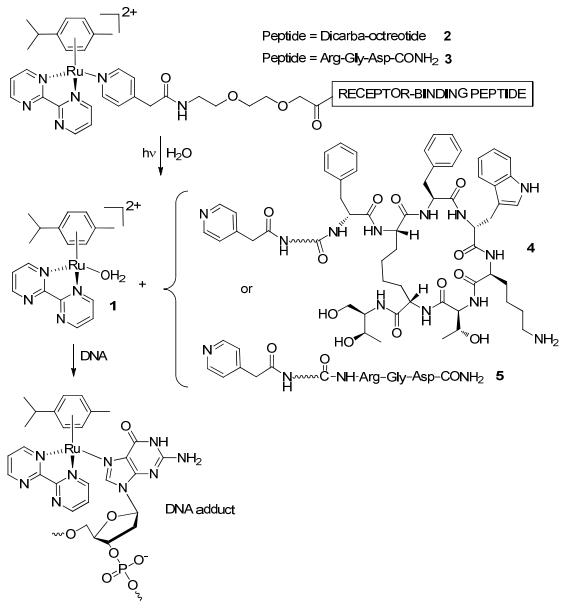

On this basis, we selected two relevant receptor-binding peptides that are expected to act as "tumor targeting devices". On the one hand, we have focused on a peptide containing the RGD (Arg-Gly-Asp) sequence to target tumour endothelial cells over healthy cells through binding to the $\alpha_V\beta_3$ and $\alpha_V\beta_5$ integrins.[9] These cell surface receptors play a predominant role in tumour-induced angiogenesis and are overexpressed on certain tumour cells during tumour growth and metastasis. On the other hand, we have chosen octreotide, a potent cyclooctapeptide agonist of the endocrine hormone somatostatin, that displays high affinity and specificity towards the sst_2 receptor subtype located in the cell membrane.[10] The fact that somatostatin receptors and, in particular sst_2, are overexpressed in various types of malignant cells, makes this peptide suitable for the specific delivery of metal-based anticancer drugs.[11] Indeed, the overexpression of the receptors for both peptides in tumors has been exploited to deliver cytotoxic agents in tumour cells as well as for molecular imaging purposes by delivering radionuclides.[3c,e,9b,12]

We report the synthesis and characterization of two novel conjugates, **2** and **3** (Scheme 1), in which a photoactivated organometallic ruthenium(II) complex is covalently bound to two receptor-binding peptides, the dicarba analogue of octreotide and the RGD tripeptide, respectively. We have investigated the effect of conjugation on photoactivation of the complexes, and competitive photo-induced reactions with DNA and peptides as potential targets. Our studies reveal not only a selectivity in ruthenation of target sites but also the photo-induced formation of multidentate coordination sites on ruthenium.

Results and Discussion

Synthesis of the ruthenium-peptide conjugates. On the basis of our previous studies on the synthesis of platinum(II)-octreotide conjugates,[3e] we choose a dicarba analogue of octreotide in which the disulfide bond is replaced by the CH_2–CH_2 linkage isostere. This modification does not substantially alter the binding affinity toward the sst_2 receptor but increases its stability in the reductive cellular environment.[13] For the synthesis of the conjugates **2** and **3**, a stepwise solid-phase approach was chosen since it allows the regioselective introduction of the ruthenium fragment at the *N*-terminal end of the peptide. This strategy has been applied successfully to the synthesis of several conjugates between peptides and coordination or organometallic complexes.[3e,3i,14] In our case, instead of synthesizing a ruthenium complex bearing a carboxylic acid function anchored at the pyridine ligand, we decided to incorporate 4-pyridyl acetic acid at the *N*-terminal end of the peptide. This ligand allows assembly of the desired ruthenium complex by displacement of the chlorido ligand in $[(\eta^6\text{-}p\text{-cym})Ru(bpm)(Cl)]^+$ or aqua ligand in the hydrolysed complex **1** (Scheme 2). A polyethyleneglycol spacer was introduced between the pyridine ligand and the peptide sequence so the ruthenium complex does not interfere with the binding of the peptide pharmacophore and to improve the aqueous solubility of the conjugate.

First, both peptides were manually assembled on a Rink amide resin using standard Fmoc-*t*Bu methodology. The suitably-protected Fmoc-amino acids were incorporated using HATU in the presence of DIPEA (octreotide) or DIPC/HOBt (RGD) as coupling reagents. In the case of octreotide, Fmoc-protected threoninol functionalized as the *p*-carboxybenzaldehyde acetal was first attached to the solid support and the two cysteines in the octreotide sequence were replaced by allyl glycine residues. On-resin ring-closing metathesis with second-generation Grubbs catalyst under microwave irradiation followed by the hydrogenation of the double bond using Wilkinson's catalyst afforded the cyclic saturated dicarba analogue of octreotide bound to the resin.[3e,13] Finally, after the incorporation of the Fmoc-protected polyethyleneglycol linker into the RGD- and octreotide-bound resins, 4-pyridyl acetic acid hydrochloride was coupled using HATU (Scheme 2).

Scheme 2. Schematic representation of the two approaches used for the synthesis of the ruthenium-octreotide conjugate 2

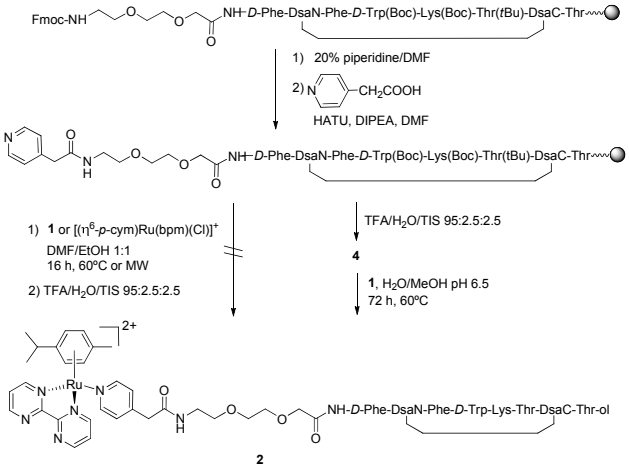

Our initial strategy for synthesis of the ruthenium conjugate involved coordination to the pyridine ligand followed by acidic treatment with TFA to cleave the conjugate from the resin and to deprotect the amino acid side chains (Scheme 2). The complex $[(\eta^6\text{-}p\text{-cym})Ru(bpm)(Cl)]^+$ as well as its aqua adduct **1** were reacted under a variety of conditions in the dark (DMF, DMF/EtOH or DCM at 60°C or under microwave irradiation) with both pyridyl-derivatized peptide-bound resins to generate the desired photoactivatable complex. Unfortunately, after treatment of the metal-peptide-bound resins either with a cocktail of TFA/H_2O/TIS 95:2.5:2.5 or with TFA/H_2O 95:5, nei-

ther ruthenium conjugate **2** nor **3** were identified in the crude products, as inferred by reversed-phase HPLC analysis and ESI and MALDI-TOF mass spectrometry. In all cases, the pyridyl-derivatized peptides **4** and **5** (Scheme 1) were identified as the main products together with the ruthenium complex **1**, which suggested that the complex was assembled on the solid-phase but that the pyridyl ligand-linker-peptide dissociated during the acidic treatment. This result prompted us to assemble the photoactivatable ruthenium complex in solution (Scheme 2).

The required pyridyl-derivatized peptides, **4** and **5**, were isolated from the peptide-bound resins by treatment with a TFA/H_2O/TIS 95:2.5:2.5 cocktail, and purification was carried out by semipreparative reversed-phase HPLC. The pyridyl-derivatized octreotide **4** was dissolved in Milli-Q water (*ca* 10 mM) and the pH was adjusted to 6.5 by addition of a few drops of a 10 mM aqueous solution of NaOH. Then, the reaction flask was protected from light with aluminium foil and the required amount of a solution of the aquated ruthenium complex **1** (4 mol eq) in a 1:1 mixture of H_2O/MeOH was added dropwise for 5 min. After 72 h at 60°C, reversed-phase HPLC analysis of the crude revealed the formation of a new product which was isolated by semipreparative HPLC and characterized by high-resolution ESI MS as the desired conjugate **2**. The same procedure was followed for the synthesis of the conjugate **3** from the pyridyl-derivatized RGD peptide **5**.

Photoactivation of the ruthenium-peptide conjugates. Next we studied the photochemical properties of the ruthenium-peptide conjugates **2** and **3** to assess how the covalent linkage of the peptides to the pyridine ligand affects the photoactivation of the ruthenium complex. First, we tested the stability of **2** and **3** in the dark (see Figure S-5). As found previously for [(η^6-*p*-cym)Ru(bpm)(py)]$^{2+}$,[6] NMR spectra revealed that both peptide-ruthenium conjugates are completely stable in aqueous solution in the dark (first at 4°C for 24 h, then at 37°C for 6 h).

The monitoring of the photoactivation processes for **2** and **3** was carried out by UV-vis and NMR spectroscopy. In both cases, an aqueous solution of the conjugate was irradiated with blue visible light (420 nm lamps) in a photo-reactor at 37°C and the UV-Vis spectra and the NMR spectra were recorded at different times. As shown in Figure 1, the ruthenium-octreotide conjugate **2** showed essentially the same behaviour to that of [(η^6-*p*-cym)Ru(bpm)(py)]$^{2+}$,[6] which indicates that the covalent attachment of the cyclic peptide to the pyridine ligand does not affect the photoactivity properties of the metal complex.

The electronic spectrum of **2** displays maxima at 256 nm, 286 nm (shoulder) and 367 nm. The presence of an isosbestic point at 309 nm is consistent with the formation of a single photoproduct. ^{1}H NMR spectra recorded at different times during the photolysis confirm the release of the octreotide-functionalized pyridine **4** and the formation of the reactive aqua species [(η^6-*p*-cym)Ru(bpm)(H_2O)]$^{2+}$ (**1**). Resonances for the metal fragment of **1** and **2** were assigned by reference to previous work on the pyridine complex.[6] No significant difference was observed in the rate and extent of photo-induced ligand release compared to the derivative [(η^6-*p*-cym)Ru(bpm)(py)]$^{2+}$ under the same light irradiation conditions. Similar results were obtained with conjugate **3** (see Figures S-7 and S-8): the photorelease of the tripeptide-functionalized pyridine **5** was observed when a solution of **3** was irradiated with blue light at 37°C.

Interestingly, no formation of peptide-metal complex adducts during light irradiation of either conjugate was evident by NMR. Such behavior is not surprising since neither octreotide nor the tripeptide sequence contain residues with proven ruthenium-binding properties (e.g. Met, His or Cys; see below).

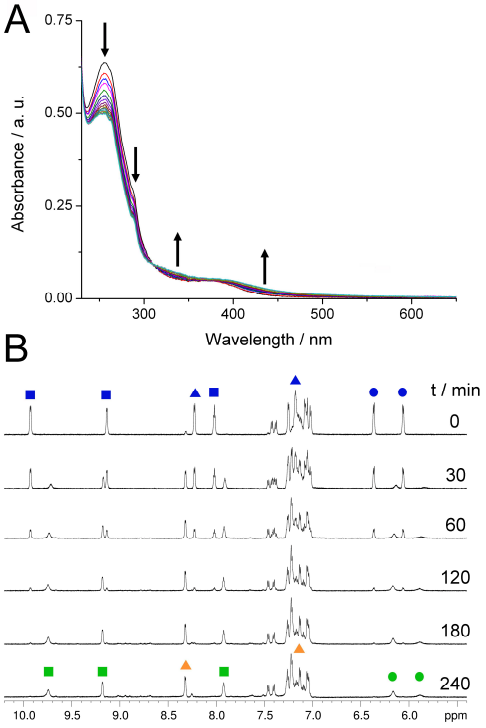

Figure 1. Photolysis (λ_{max} = 420 nm, 37°C) of **2** in aqueous solution followed by (A) UV-vis and (B) ^{1}H NMR spectroscopy. UV-vis spectra were collected at t = 0 min (black curve), every 20 min of irradiation for the first hour and every 30 min for the next 7 h; ^{1}H NMR spectra were collected at t = 0 min (B, top) and every 30 min of irradiation up to 4 h. Assignments: blue = **2**, green = **1**, ■ = bpm, ▲ = py, ● = *p*-cym. Resonances of the released pyridine functionalized with the octreotide peptide are indicated with orange ▲.

DNA ruthenation by photoactivated conjugates. DNA is a potential target for cytotoxic piano-stool Ru(II) arene complexes.[8] Therefore we investigated the ability of photoactivated ruthenium-peptide conjugates to ruthenate both the model DNA nucleobase 9-ethylguanine (9-EtG) and two short DNA sequences, $^{5'}$dCATGGCT and $^{5'}$dAGCCATG, under visible light irradiation. First 9-ethylguanine was added to an irradiated (480 min) solution of **2** (3:1 mol ratio) and incubated at 37°C. As shown in Figure 2, **1** binds 9-EtG over time to give a **1**-9-EtG adduct. A new set of signals appeared in the aromatic region and a 2D NOESY cross peak between the *H8* of the coordinated 9-EtG and the 2,2'-CH bpm proton was detected (see also Figure S-6). Similar results were obtained for the RGD conjugate **3**. The reactive aqua species **1** photoreleased from the RGD-functionalized pyridine also coordinated to 9-EtG (see Figure S-9). These results demonstrate that functionalization of the pyridine ligand in the ruthenium(II) arene complex [(η^6-*p*-cym)Ru(bpm)(py)]$^{2+}$ with small-to-medium-sized peptides does not adversely affect the photoactivation process nor the interaction of the photoreleased reactive aqua species **1** with a model G nucleobase.

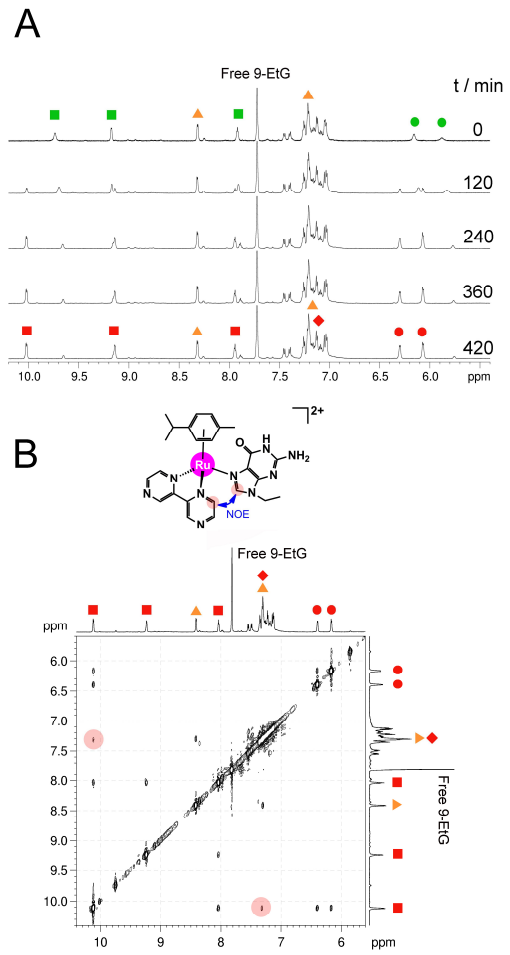

Figure 2. Reaction between 9-EtG and an irradiated solution (λ_{max} = 420 nm, 240 min, 37°C) of octreotide conjugate **2**. (A) Aromatic region of the ^{1}H NMR spectrum during the course of the reaction. Spectra were collected at t = 0 min (A, top) and every 60 min up to 7 h. (B) 2D ^{1}H-^{1}H NOESY NMR spectrum after 480 min of reaction. Green = **1**, red = **1**-9-EtG adduct; ■ = bpm, ▲ = py, ● = *p*-cym. Resonances of the released pyridine functionalized with the octreotide peptide are indicated with orange ▲ and coordinated 9-EtG (*H8*) with red ♦.

Next we studied the short synthetic oligonucleotide $^{5'}$dCATGGCT which contains a GpG sequence, the target for the anticancer drug cisplatin.[1] This DNA fragment gives the expected platinum 1,2-intrastrand GG chelates upon reaction either with cisplatin, [Pt(en)Cl$_2$] or the dichloroplatinum(II) conjugate of a dicarba analogue of octreotide.[3e,15]

First, $^{5'}$dCATGGCT was added to an irradiated (8 h) solution of conjugate **2** (5:1 mol ratio) and incubated overnight. Reversed-phase HPLC analysis with on-line UV detection showed the presence of two new peaks with higher retention time than the parent oligonucleotide (R_t = 18.3 and 19.1 min; relative ratio 0.85:1, respectively; see Figure 3), attributable both to the hydrophobicity of the ruthenating fragment, {(η^6-*p*-cym)Ru(bpm)}$^{2+}$, as well as to the position of the ruthenation in the sequence. High resolution ESI and MALDI-TOF MS analysis of the two products confirmed the formation of isomeric ruthenated DNA adducts in which a single ruthenium fragment, {(η^6-*p*-cym)Ru(bpm)}$^{2+}$, was coordinately bound to the DNA chain (**6a-b**) (Scheme 3). The position of the ruthenium adduct was determined by MS analysis of the products after enzymatic digestion with 5´- and 3´-exonucleases (bovine spleen and snake venom phosphodiesterases, respectively).[16] As expected, the aqua ruthenium complex reacted exclusively with both guanines, thus paralleling the reactivity towards the model nucleobase 9-EtG. The high affinity of similar ruthenium(II) arene complexes, such as [(η^6-*p*-cym)Ru(en)Cl]$^+$, for the *N7* position of guanine has been observed previously for different oligonucleotide sequences.[17] This strong preference for the *N7* site of guanine over the other DNA nucleobases has also been demonstrated in the case of the aqua complex [(η^6-benzene)Ru(en)(OH$_2$)]$^{2+}$ by using computation either in the gas or in aqueous solution.[18]

As a control, the reaction between $^{5'}$dCATGGCT and [(η^6-*p*-cymene)Ru(bpm)(OH$_2$)]$^{2+}$ was carried out in aqueous solution to confirm that the latter species is responsible for the formation of the monofunctional ruthenium adducts. Indeed, only **6a** and **6b** were detected by reversed-phase HPLC analysis in a similar ratio as in the previous experiment. In addition, no reaction was observed when conjugate **2** and $^{5'}$dCATGGCT were incubated for 16 h at ambient temperature in the dark (Figure S-10), which suggests that direct displacement of the pyridyl-derivatized peptide by guanines from the DNA cannot readily take place. These results confirm that photoreleased aqua complex **1** is the ruthenating species and that the peptide does not interfere in the DNA ruthenation step.

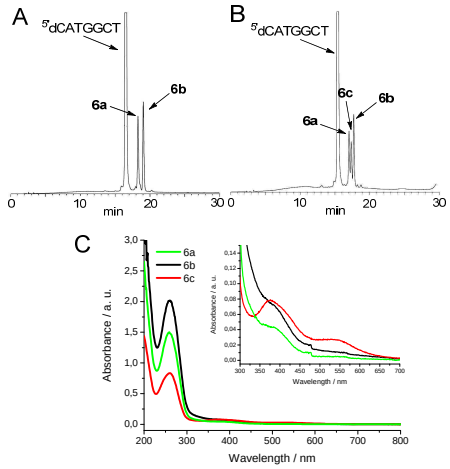

Figure 3. Reversed-phase HPLC traces for (A) the reaction between $^{5'}$dCATGGCT and an irradiated solution of conjugate **2** (8 h, 37°C) after a further 15 h at ambient temperature and (B) the *in situ* reaction between $^{5'}$dCATGGCT and conjugate **2** after 9 h of irradiation at 37°C. (C) Absorption spectra of the isolated adducts **6a** (green), **6b** (black) and **6c** (red). The inset shows an expansion of the 300-700 nm region.

It is interesting that **1** is able to ruthenate both guanines of the GG sequence in the oligonucleotide, which is a different trend from that previously described for monofunctional platinum(II) complexes. For example, {Pt(dien)}$^{2+}$, a model for monofunctional adducts of cisplatin, exclusively reacts with the 5'G nucleobase in the $^{5'}$dCATGGCT sequence.[15] In addition, it seems that there is no preference for any of the guanines in the GG-containing oligonucleotide. This is also a different trend compared to cisplatin, for which it has been reported that there is a slight preference for 3'G monofunctional adducts in GG sequences.[19]

Once the ability of photoreleased **1** to ruthenate DNA had been demonstrated, we investigated whether the monofunctional adducts **6a** (G^5-Ru) and **6b** (G^4-Ru) would also be formed when conjugate **2** was photoactivated in the presence of the oligonucleotide. Thus, an aqueous solution of conjugate **2** together with 5 mol eq of $^{5'}$dCATGGCT was irradiated with blue light at 37°C for 9 h. Interestingly, reversed-phase HPLC analysis showed the presence of a new peak (R_t = 18.6 min; see Figure 3B) together with two peaks corresponding to adducts **6a** and **6b**. The UV-vis absorption spectrum of this new compound **(6c)** contained some different features to those of **6a** and **6b** (Figure 3C), notably the appearance of a broad band near 550 nm. These changes in the absorption spectrum suggested that the environment of the metal might had been substantially modified.

To our surprise, HR ESI and MALDI-TOF MS analysis of the new product **6c** revealed the formation of a DNA adduct in which the *p*-cymene ligand had been displaced from ruthenium and the single ruthenium fragment, $\{Ru(bpm)\}^{2+}$, was bound to the oligonucleotide. The fact that this product is formed only when the mixture of the conjugate and the oligonucleotide is continuously irradiated suggests that the loss of the *p*-cymene ligand is triggered by irradiation with visible light and perhaps driven by formation of a GG chelate. It is important to note that NMR data from the photoactivation experiments with conjugates **2** and **3** appear to rule out the possibility that the loss of the arene ligand takes place from the photoreleased aqua species **1** as a consequence of the irradiation. Therefore, we hypothesize that **6c** is generated from both monofunctional ruthenium adducts **(6a** and **6b)** and that the formation of a more stable adduct **(6c)** is the driving force of the photo-induced release of *p*-cymene. The UV-vis spectra of this compound (Figure 3C) is in good agreement with the loss of the arene ligand.

Two control experiments confirmed this hypothesis. First, all three adducts were obtained when a mixture of $^{5'}$dCATGGCT and $[(\eta^6\text{-}p\text{-cymene})Ru(bpm)(OH_2)]^{2+}$ was irradiated at 37°C for 7 h (Figure S-11). Second, adduct **6c** was generated when isolated monofunctional ruthenium adducts **(6a-b)** were photolysed. Interestingly, a mixture of the three adducts was always obtained from each monofunctional adduct upon irradiation but adduct **6c** remained unaltered (Figure S-12). These results confirm the higher stability of adduct **6c** compared to that of **6a-b**. Hence, continuous *in situ* irradiation of monofunctional ruthenated adducts triggers either deruthenation to regenerate the DNA strand or the release of the *p*-cymene ligand to give the most stable adduct, **6c**. These observations are also in good agreement with MS results since the ionization conditions employed during MALDI-TOF MS analysis caused a large amount of ligand loss (both *p*-cymene and bpm) from adducts **6a** and **6b** in comparison with that observed for adduct **6c**. However, no significant loss of the ligands was observed during HR ESI MS analysis (see Figures S-13-S-16).

In order to determine the position of the ruthenating fragment $\{Ru(bpm)\}^{2+}$ in the oligonucleotide chain, **6c** was submitted to enzymatic digestion with exo- and endo-nucleases. MS analysis after treatment with 5´ and 3´ phosphodiesterases as well as with nuclease S1 confirmed that G^4 and G^5 are involved in ruthenium coordination (Scheme 3).

Scheme 3. Contrasting pathways for photo-induced reactions of octreotide conjugate **2** with $^{5'}$dCATGGCT. Left branch: pre-irradiated followed by addition of the oligonucleotide. Right branch: irradiation of a mixture of **2** and the oligonucleotide. In the former only monofunctional adducts are formed, whereas the latter provides a pathway to bifunctional adducts via arene release

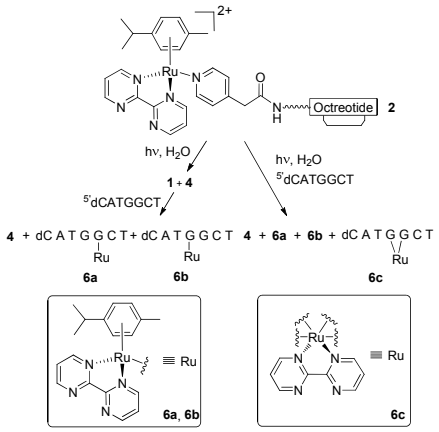

Since the irradiation of photoactivated ruthenium(II) arene complexes or their conjugates with carrier molecules, such as peptide conjugates **2** and **3**, would be performed directly in the tumor, the formation of different types adducts with DNA such as **6a-c** might have important biological consequences. For example, it has been demonstrated that adducts formed when DNA is treated with $[(\eta^6\text{-arene})Ru(en)Cl]^+$ are more difficult for enzymes to repair than the bifunctional adducts formed by cisplatin.[20] In the present case, besides typical monofunctional ruthenium adducts **(6a-b)**, *in situ* irradiation triggers ruthenation of DNA through the coordination of both guanines **(6c)**. The release of the η^6-arene ligand creates three potentially reactive sites around the metal for interaction with DNA (or RNA) or other biomolecules (see below). As a consequence, this allows the formation of adducts with different structures compared to the typical monofunctional adducts formed by N,N-chelated ruthenium arene anticancer complexes or the classical 1,2-intrastrand cross-links formed by square-planar cisplatin. This difference is likely to affect protein recognition of the ruthenated lesions and hence their repair.

Arene loss followed by binding to oligonucleotides and proteins has been previously described for some classical ruthenium(II) arene complexes, such as $[(\eta^6\text{-}p\text{-cym})Ru(pta)Cl_2]$ and $[(\eta^6\text{-}C_6H_5CF_3))Ru(pta)Cl_2]$.[21] In addition, we have previously found that the dinuclear complex $[\{(\eta^6\text{-indan})RuCl\}_2(\mu\text{-}2,3\text{-dpp})]^{2+}$ undergoes indan loss via an oxygen-independent pathway when irradiated at 365 nm UVA.[22] However, analogous complexes containing *p*-cymene or hexamethylbenzene do not undergo arene loss upon irradiation, which can be attributed to their stronger donor character. The highly reactive ruthenium species created by the photoactivation of $[\{(\eta^6\text{-indan})RuCl\}_2(\mu\text{-}2,3\text{-dpp})]^{2+}$ are also capable of forming both mono- and bifunctional adducts with DNA. This is consistent with the fact that the release of *p*-cymene from **1** alone does not occur under irradiation with visible light but is photo-induced from the monofunctional DNA adducts **6a-b** to give **6c**.

Next we studied photo-induced ruthenation of an oligonucleotide with two G bases in non-adjacent positions, $^{5'}$dAGCCATG. Since the generation of non-classical ruthen-

ated adducts as a consequence of the photo-driven arene loss, such as **6c**, might have important implications for the biological activity of photoactivated ruthenium(II) arene complexes because of their multidentate nature, we wondered whether the formation of these adducts is exclusively related to GG-containing sequences in DNA or their formation might be more general.

Again, irradiation with visible light of an aqueous solution of conjugate **2** together with 5´dAGCCATG led to three main products (**7a-c**) (see Figure S-17). HR MALDI-TOF MS analysis together with enzymatic digestion revealed that in the two products with higher retention times than the parent oligonucleotide, **7b** and **7c**, the fragment $\{(\eta^6\text{-}p\text{-cym})Ru(bpm)\}^{2+}$ was bound to G^7 and G^2, respectively (see Scheme 4 and Figure S-18). Regarding product **7a**, whose retention time is surprisingly lower than that of 5´dAGCCATG (14.0 min *vs* 15.2 min), HR MALDI-TOF MS analysis indicated that the *p*-cymene ligand had been lost, as previously found for **6c**. Again, enzymatic digestion with 5´- and 3´-exonucleases revealed that both guanines are involved in coordination to the ruthenating species, $\{Ru(bpm)\}^{2+}$. In addition, a short treatment (10 min) of **7a** with nuclease S1 afforded, among others, a product with an *m/z* ratio 18 units higher than that of the parent compound; this corresponds to the cleavage of a phosphodiester bond between both guanines with the subsequent addition of a water molecule. The overall data from enzymatic digestions confirm the cyclic nature of **7a** and that only guanines are involved in the coordination to the ruthenating fragment (Scheme 4). Hence, these results demonstrate again the high preference of the photoreleased species $[(\eta^6\text{-}p\text{-cymene})Ru(bpm)(OH_2)]^{2+}$, for guanines and that the phototriggered arene release allows their ligation via $\{Ru(bpm)\}^{2+}$, even if they are located far from each other in a DNA sequence. The formation of such adducts is expected to alter DNA (or RNA) structure dramatically and, consequently, to interfere with cell repair mechanisms.

Photo-induced reaction of ruthenium-octreotide conjugate with Phac-His-Gly-Met-linker-p^5´dCATGGCT. As seen above, the aqua species **1** photoreleased from conjugate **2** is able to ruthenate DNA *in situ*. However, in a cell there would be competition for binding from peptides and proteins. To investigate such competition we studied next reaction of a peptide-oligonucleotide hybrid, Phac-His-Gly-Met-linker-p^5´dCATGGCT, in which the oligonucleotide sequence is covalently attached to a tripeptide that contains the two residues most prone to form strong complexes with platinum and ruthenium compounds, methionine and histidine. This bioconjugate was synthesized using solid-phase procedures[23] and it has been previously used in platination studies both with cisplatin and its inactive isomer transplatin.[15,16a]

An aqueous solution of conjugate **2** and Phac-His-Gly-Met-linker-p^5´dCATGGCT (1 mol eq) was irradiated with visible light at 37ºC for 9 h. HPLC analysis revealed the formation of three main products (**8a-c**; see Scheme 4) with higher retention times than the parent bioconjugate (R_t = 16.0, 16.9 and 17.1 min; relative ratio 0.95:0.75:1, respectively; see Figure 4). Similarly to 5´dCATGGCT, the reaction between Phac-His-Gly-Met-linker-p^5´dCATGGCT and aqua adduct **1** afforded only two products, **8b** and **8c**. HR MALDI-TOF MS analysis of **8b** and **8c** confirmed that the fragment $\{(\eta^6\text{-}p\text{-cym})Ru(bpm)\}^{2+}$ was bound to the bioconjugate in both cases (see Figure S-19).

Scheme 4. Formation of ruthenium adducts after irradiation of **2** in the presence of the oligonucleotide (left) or the peptide-oligonucleotide hybrid (right).

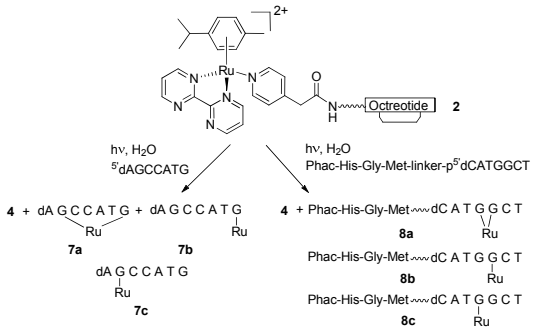

Reaction of **8b-c** with an aqueous solution of H_2O_2 (5%) led to oxidation of the methionine thioether sulphur (to the sulfoxide, *m/z* 16 units higher)[16] suggesting that the Met sulphur was unprotected and not ruthenated. In addition, removal of the fragment Phac-His-Gly-Met after digestion with pronase indicated no coordination to the imidazole ring of the histidine residue.[16] Finally, treatment with snake venom phosphodiesterase suggested that the G^5 nucleobase was ruthenated in **8b** and the G^4 in **8c** (fragments pCpT and pGpCpT were removed, respectively), thus reproducing the coordination pattern found in adducts **6a-b** (see Schemes 3 and 4).

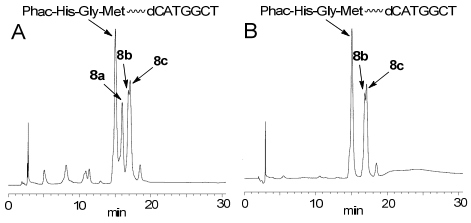

Figure 4. Reversed-phase HPLC traces for the *in situ* reaction between (A) Phac-His-Gly-Met-linker-p^5´dCATGGCT and conjugate **2** after 9 h of irradiation at 37ºC, and (B) reaction between Phac-His-Gly-Met-linker-p^5´dCATGGCT and the ruthenium aqua adduct **1** after 15 h at room temperature.

Regarding adduct **8a**, formed only during continuous irradiation, HR MALDI-TOF MS analysis revealed the loss of the *p*-cymene ligand which, as previously found with 5´dCATGGCT and 5´dAGCCATG, was a consequence of *in situ* irradiation with visible light. This is in good agreement with the UV-vis spectra of this compound in comparison with that of **8b-c** (see Figure S-20). Again, treatment with H_2O_2 and digestion with pronase ruled out coordination of $\{Ru(bpm)\}^{2+}$ to the peptide fragment. Enzymatic digestion with the 3´-exonuclease and with nuclease S1 revealed the formation of a chelate with both guanines (Scheme 4), thus confirming again the strong preference of this ruthenium complex for these nucleobases.

Two important conclusions can be drawn from these experiments. First, the photoreleased aqua complex **1** does not react with the histidine nor methionine side chains in the peptide, but exclusively with the oligonucleotide portion to generate monofunctional adducts at both guanine nucleobases (**8b-c**). Second, *in situ* irradiation also induces the loss of the *p*-cymene ligand from the monofunctional adducts to generate a chelate (**8a**) in which $\{Ru(bpm)\}^{2+}$ is bound to both guanines. Hence,

the behaviour of Phac-His-Gly-Met-linker-p[5']dCATGGCT demonstrates the preference of the photoactivated ruthenium(II) arene complex for DNA over peptides containing His *N*- and Met *S*-donor ligands. In addition, we observe photo-induced arene release from DNA monofunctional adducts and the formation of a chelate involving two guanines (**8a**), equivalent to the course of the reaction observed for [5']dCATGGCT (**6c**) and [5']dAGCCATG (**7a**). Perhaps surprisingly neither histidine nor methionine appear to bind to either of the two vacant coordination positions on the ruthenium(II) in **8a**. This might be a consequence of steric hindrance because of the covalent attachment between the peptide and the oligonucleotide chain. To check this possibility, we irradiated conjugate **2** in the presence of [5']dCATGGCT (1 mol eq) and the peptide Ac-His-Gly-Met-NH_2-(1 mol eq) with visible light at 37°C for 7 h. Surprisingly, only monofunctional adducts **6a,b** and chelate **6c** were formed, as inferred by HPLC and MS analysis (Figure S-21). No evidence for the interaction between the tripeptide and photoreleased **1** or adduct **6c** was obtained from these experiments. Further investigations will be necessary to determine whether other potential biological ligands can form ternary adducts with ruthenated DNA as a consequence of *in situ* irradiation with visible light.

Conclusion. In summary, we have described a straightforward methodology for the conjugation of a photoactivated ruthenium(II) arene complex to receptor-binding peptides such as a dicarba analogue of octreotide and the RGD sequence. UV-vis spectroscopy and NMR data have demonstrated that both conjugates are completely stable in aqueous solution in the dark but that the corresponding pyridyl-derivatized peptides are selectively photodissociated upon irradiation with visible light, providing an elegant and innovative mechanism for the activation of such potential anticancer agents. Importantly, the release of the aqua complex from the conjugate, namely $[(\eta^6\text{-}p\text{-cym})Ru(bpm)(H_2O)]^{2+}$, is not influenced by the covalent attachment of the peptides to the pyridine ligand. In addition, this reactive species is able to bind a DNA nucleobase model, 9-ethylguanine, as well as the two guanines in two DNA sequences, [5']dCATGGCT and [5']dAGCCATG, as inferred by NMR and enzymatic digestion in combination with MS. This behavior was reproduced with Phac-His-Gly-Met-linker-p[5']dCATGGCT since two monofunctional adducts on both guanine nucleobases were also formed. Surprisingly, when the ruthenium-octreotide conjugate was irradiated in the presence of both oligonucleotides or the peptide-oligonucleotide hybrid, a new ruthenated product involving coordination to the two guanines was formed as a consequence of the loss of the *p*-cymene ligand. The formation of this adduct with a bidentate binding mode is phototriggered from monofunctional adducts on guanines, even if they are located far from each other in the DNA sequence. Since irradiation will be performed *in situ* in the tumor, the generation of such non-classical adducts might have important implications for cellular repair mechanisms. In the experiments with Phac-His-Gly-Met-linker-p[5']dCATGGCT, no interaction was found with the peptide fragment, even in the adduct in which *p*-cymene had been lost, which indicates a higher preference of this photoactivated ruthenium(II) complex for guanines on DNA (or RNA) over other potential biological ligands such as histidine or methionine amino acids.

To the best of our knowledge, this work provides the first example of a potential ruthenium-based anticancer agent with a double mechanism of selectivity. First, the receptor-binding peptide can act as a "tumour targeting device", thereby directing the ruthenium pro-drug to the cancer cell via specific receptors that are overexpressed on the membrane of certain tumoural cells. Second, direct irradiation with visible light in the tumor will promote photodissociation of the ruthenium aqua complex, $[(\eta^6\text{-}p\text{-cym})Ru(bpm)(H_2O)]^{2+}$, from the peptide. Our experiments demonstrate that this reactive species might react preferably with DNA compared to proteins and that, under irradiation, classical monofunctional ruthenium adducts on guanine nucleobases might be transformed into more resistant adducts. This dual mechanism of selectivity and activity will not only contribute to reducing toxic side-effects associated with metal-based anticancer drugs, but also has the potential to produce novel lesions on DNA and therefore a novel mechanism of anticancer activity with a low cross-resistance to other drugs. Work is in progress to evaluate the biological activity of the conjugates toward several cancer cell lines as well as to extend this strategy to delivering other biomolecules and photoactive metal complexes.

Experimental Section

Materials and Methods. Unless otherwise stated, common chemicals and solvents (HPLC grade or reagent grade quality) were purchased from commercial sources and used without further purification. Fmoc-protected amino acids, resins and coupling reagents for solid-phase synthesis were obtained from Novabiochem, Bachem or Iris Biotech. Milli-Q water was directly obtained from a Milli-Q system equipped with a 5000-Da ultrafiltration cartridge. Solid-phase syntheses were performed manually in a polypropylene syringe fitted with a polyethylene disc. The syntheses of $[(\eta^6\text{-}p\text{-cym})Ru(bpm)(Cl)][PF_6]$ and $[(\eta^6\text{-}p\text{-cym})Ru(bpm)(H_2O)][PF_6]_2$ were carried out following previously reported procedures.[6]

A) NMR spectroscopy: NMR spectra were recorded at 25°C on a Varian Gemini 200 or 300 MHz and Varian Mercury 400 MHz spectrometers using deuterated solvents. Tetramethylsilane (TMS) was used as an internal reference (δ 0 ppm) for ^1H spectra recorded in $CDCl_3$ and the residual signal of the solvent (δ 77.16 ppm) for ^{13}C spectra. In the case of irradiation experiments, NMR spectra were acquired on a Bruker AV II 700 MHz spectrometer and ^1H NMR signals were referenced to dioxane as an internal reference (δ 3.75 ppm). A standard phase sensitive NOESY pulse sequence was employed with 0.8 s mixing time. Solutions of 400 μM **2** and **3** were employed for photolysis studies.

B) Mass spectrometry: High resolution MALDI-TOF mass spectra were recorded on a 4800 Plus MALDI-TOF/TOF spectrometer (Applied Biosystems) in the positive mode using 2,4-dihidroxybenzoic acid as a matrix. ESI mass spectra (ESI-MS) were recorded on a Micromass ZQ instrument with a single quadrupole detector coupled to an HPLC. High resolution electrospray mass spectra (HR ESI-MS) were obtained either on a BrukerMaXis UHR-TOF or on an Agilent 1100 LC/MS-TOF instrument.

C) UV-vis absorption spectroscopy: UV-vis absorption spectra were recorded on a Cary 50-Bio spectrophotometer using 1-cm path-length quartz cuvettes (0.5 mL) and a PTP1 Peltier temperature controller. Spectra were recorded at *ca* 37°C in double distilled water from 800 to 230 nm, and were processed using UV-Winlab software for Windows 95. 200 μM solution of **2** and **3** were employed for photolysis studies.

D) Irradiation experiments: The light source was a Luzchem LZC-ICH2 illuminator (photo-reactor) oven using LZC-420 (blue light) lamps, with no other sources of light filtration. The photo-reactor operated at 420 nm (λ_{max}) with temperature controller at 37°C and power level of *ca* 1 J cm^{-2} h^{-1}. The power levels were monitored using the appropriate probe window, calibrated with an OAI power meter from Optical Associates, Inc.

E) HPLC analysis and purification: Analytical reversed-phase HPLC analyses were carried out on a Jupiter Proteo C_{18} column (250 x 4 mm, 5 μm, flow rate: 1 mL/min), using linear gradients of 0.045% TFA in H_2O (solvent A) and 0.036% TFA in ACN (solvent B). Purification was carried out on a Jupiter Proteo semipreparative column (250 x 10 mm, 10 μm, flow rate: 4 mL/min), using linear gradients of 0.1% TFA in H_2O (solvent A) and 0.1% TFA in ACN (solvent B). HPLC-MS analysis was performed using a Micromass ZQ mass spectrometer equipped with an electrospray source and a single quadrupole detector coupled to a Waters 2695 HPLC (photodiode array detector). Elution was performed on a GraceSmart C_{18} column (150 x 2.1 mm, 5 μm, flow rate: 0.25 ml/min) with linear gradients of H_2O and ACN containing both solvents 0.1% formic acid.

Synthesis of the ruthenium-peptide conjugates 2 and 3. *A) Octreotide-ruthenium conjugate 2*: 8 μmol of the pyridyl-derivatized octreotide **4** were dissolved in 800 μL of Milli-Q water and the pH was adjusted to 6.5 by adding a few μL of a 10 mM aqueous solution of NaOH. The Eppendorf tube was protected from light by covering it with aluminium foil and 1.5 mL of a 20 mM solution of $[(\eta^6\text{-}p\text{-cym})Ru(bpm)(H_2O)][PF_6]_2$ (3.75 eq) in H_2O/MeOH 1:1 were added dropwise for 5 min. The reaction mixture was kept at 60°C for 72 h protected from the light. Reversed-phase HPLC analysis revealed the formation of a new peak (87%) which corresponds to the conjugate **2**, as inferred by ESI MS. After purification by semipreparative HPLC (gradient: 20 to 60% in 30 min, R_t= 12.6 min) and lyophilisation, the product was obtained as a yellow foam (28% global yield). Characterization: R_t= 13.7 min (analytical gradient: 20 to 60% in 30 min); HR ESI-MS, positive mode: *m/z* 820.3584 (calcd mass for $C_{82}H_{106}N_{16}O_{14}Ru$ $[M]^{2+}$: 820.3559), 547.2400 (calcd mass for $C_{82}H_{107}N_{16}O_{14}Ru$ $[M+H]^{3+}$: 547.2399).

B) RGD-ruthenium conjugate 3: 1 μmol of the pyridyl-derivatized RGD peptide **5** was dissolved in 450 μL of Milli-Q water and the pH was adjusted to 6.8 by adding a few μL of a 10 mM aqueous solution of NaOH. The Eppendorf tube was protected from light by covering it with aluminium foil and 1 mL of a 20 mM solution of $[(\eta^6\text{-}p\text{-cym})Ru(bpm)(H_2O)][PF_6]_2$ (20 eq) in H_2O/MeOH 1:1 was added dropwise over 5 min. The reaction mixture was kept at 60°C for 48 h protected from the light. Reversed-HPLC analysis revealed the formation of a new peak (65%) which corresponds to the conjugate **3**, as inferred by ESI MS. After purification by semipreparative HPLC (gradient: 0 to 40% in 30 min, R_t= 18.2 min) and lyophilisation, the product was obtained as a yellow foam (29% global yield). Characterization: R_t= 15.3 min (analytical gradient: 0 to 50% in 30 min); HR ESI-MS, positive mode: *m/z* 501.6795 (calcd mass for $[M]^{2+}$ $C_{43}H_{59}N_{13}O_9Ru$: 501.6801), 334.7887 (calcd mass for $C_{43}H_{60}N_{13}O_9Ru$ $[M+H]^{3+}$: 334.7893).

DNA binding studies. *A) In situ experiments:* The required volume of an aqueous solution of conjugate **2** was mixed with the required volume of an aqueous solution of the oligonucleotide, $^{5'}$dCATGGCT (5 mol eq) or $^{5'}$dAGCCATG (1 mol eq), or the peptide-oligonucleotide hybrid (1 mol eq), Phac-His-Gly-Met-linker-p$^{5'}$dCATGGCT. The solutions were 100 μM in **2**. Ruthenation reactions were carried out at 37°C in a quartz cuvette under visible light irradiation. The light source was a Philips Belgium A3 Master HPI-T Plus 400W visible lamp and a 1 M aqueous solution of $NaNO_2$ was used as a filter to cut off the UV-light and ensure the appropriate wavelength range (> 400 nm).

B) DNA binding to pre-irradiated samples: An aqueous solution of conjugate **2** (100 μM) was irradiated for 9 h at 37°C. Then, the required volume of an aqueous solution of the oligonucleotide (5 mol eq) or the peptide-oligonucleotide hybrid (1 mol eq) was added and the reaction mixture was incubated protected from light at 37°C overnight.

C) Control experiments with 1: The required volume of a 20 mM solution of $[(\eta^6\text{-}p\text{-cym})Ru(bpm)(H_2O)][PF_6]_2$ in H_2O/MeOH 1:1 was mixed with the required volume of an aqueous solution of $^{5'}$dCATGGCT (5 mol eq) or Phac-His-Gly-Met-linker-p$^{5'}$dCATGGCT (1 mol eq). The solutions were 100 μM in **1**. Ruthenation reactions were carried out at room temperature overnight and protected from light.

D) Analysis and characterization of the ruthenium adducts: The evolution of the reactions was monitored by reversed-phase HPLC on Kromasil C_{18} columns (250 x 4.6 mm, 10 μm, flow rate: 1 mL/min), using linear gradients of aqueous triethylammonium acetate (0.05 M) (solvent A) and ACN/H_2O 1:1 (solvent B). Ruthenium adducts were isolated after several HPLC runs by using analytical separation conditions. HR MALDI-TOF MS analysis was carried out in the negative mode using 2,4,6-trihidroxyacetophenone matrix with ammonium citrate as an additive. Enzymatic digestions with 5'- and 3'-exonucleases (bovine spleen and snake venom phosphodiesterases, respectively), nuclease S1 and pronase were performed as previously described.[16]

*D.1) Adduct $^{5'}$dCATG**G**CT-[(η^6-p-cym)Ru(bpm)]$^{2+}$ **6a***: R_t= 18.3 min (gradient: 5 to 45% in 30 min). HR ESI-MS, negative mode: *m/z* 1242.7169 (calcd mass for $C_{86}H_{103}N_{29}O_{41}P_6Ru$ $[M\text{-}4H]^{2-}$: 1242.7168), *m/z* 828.1432 (calcd mass for $C_{86}H_{102}N_{29}O_{41}P_6Ru$ $[M\text{-}5H]^{3-}$: 828.1419), *m/z* 620.8536 (calcd mass for $C_{86}H_{101}N_{29}O_{41}P_6Ru$ $[M\text{-}6H]^{4-}$: 620.8545). MALDI-TOF-MS, negative mode: *m/z* 2486.8 (calcd mass for $C_{86}H_{104}N_{29}O_{41}P_6Ru$ $[M\text{-}3H]^-$: 2486.44), *m/z* 2352.7 (calcd mass for $C_{76}H_{90}N_{29}O_{41}P_6Ru$ $[M\text{-}(p\text{-cym})\text{-}3H]^-$: 2352.33), *m/z* 2329.7 (calcd mass for $C_{78}H_{98}N_{25}O_{41}P_6Ru$ $[M\text{-bpm-}3H]^-$: 2328.38). MALDI-TOF-MS after digestion with snake venom phosphodiesterase: *m/z* 1759.9 (-pCpT) (calcd mass for $C_{57}H_{65}N_{24}O_{28}P_4Ru$ $[M\text{-}(p\text{-cym})\text{-}3H]^-$: 1759.24), *m/z* 1501.8 (-pCpT) (calcd mass for $C_{49}H_{61}N_{20}O_{28}P_4$ $[M\text{-}(p\text{-cym})\text{-Ru-bpm-}H]^-$: 1501.29). MALDI-TOF-MS after digestion with bovine spleen phosphodiesterase: *m/z* 1580.9 (-CpApTp) (calcd mass for $C_{57}H_{67}N_{19}O_{23}P_3Ru$ $[M\text{-}3H]^-$: 1580.29), *m/z* 1446.8 (-CpApTp) (calcd mass for $C_{47}H_{53}N_{19}O_{23}P_3Ru$ $[M\text{-}(p\text{-cym})\text{-}3H]^-$: 1446.18), *m/z* 1422.8 (-CpApTp) (calcd mass for $C_{49}H_{61}N_{15}O_{23}P_3Ru$ $[M\text{-bpm-}3H]^-$: 1422.23), *m/z* 1188.7 (-CpApTp) (calcd mass for $C_{39}H_{49}N_{15}O_{23}P_3$ $[M\text{-}(p\text{-cym})\text{-Ru-bpm-}H]^-$: 1188.24), *m/z* 859.2 (-CpApTpGp) (calcd mass for $C_{29}H_{37}N_{10}O_{17}P_2$ $[M\text{-}(p\text{-cym})\text{-Ru-bpm-}H]^-$: 859.18).

*D.2) Adduct $^{5'}$dCAT**G**GCT-[(η^6-p-cym)Ru(bpm)]$^{2+}$ **6b***: R_t= 19.1 min (gradient: 5 to 45% in 30 min). HR ESI-MS, negative mode: *m/z* 1242.7126 (calcd mass for $C_{86}H_{103}N_{29}O_{41}P_6Ru$ $[M\text{-}4H]^{2-}$: 1242.7168), *m/z* 828.1422 (calcd mass for $C_{86}H_{102}N_{29}O_{41}P_6Ru$ $[M\text{-}5H]^{3-}$: 828.1419), *m/z* 620.8560 (calcd mass for $C_{86}H_{101}N_{29}O_{41}P_6Ru$ $[M\text{-}6H]^{4-}$: 620.8545). MALDI-TOF-MS, negative mode: *m/z* 2486.0 (calcd mass for $C_{86}H_{104}N_{29}O_{41}P_6Ru$ $[M\text{-}3H]^-$: 2486.44), *m/z* 2352.9 (calcd mass for

$C_{76}H_{90}N_{29}O_{41}P_6Ru$ [M-(*p*-cym)-3H]$^-$: 2352.33), *m/z* 2328.9 (calcd mass for $C_{78}H_{98}N_{25}O_{41}P_6Ru$ [M-bpm-3H]$^-$: 2328.38). MALDI-TOF-MS after digestion with snake venom phosphodiesterase: *m/z* 1430.8 (-pGpCpT) (calcd mass for $C_{47}H_{53}N_{19}O_{22}P_3Ru$ [M-(*p*-cym)-3H]$^-$: 1430.19), *m/z* 1407.8 (-pGpCpT) (calcd mass for $C_{49}H_{61}N_{15}O_{22}P_3Ru$ [M-bpm-3H]$^-$: 1406.24), *m/z* 1172.7 (-pGpCpT) (calcd mass for $C_{39}H_{49}N_{15}O_{22}P_3$ [M-(*p*-cym)-Ru-bpm-H]$^-$: 1172.24). MALDI-TOF-MS after digestion with bovine spleen phosphodiesterase: *m/z* 1885.1 (-CpAp) (calcd mass for $C_{67}H_{80}N_{21}O_{30}P_4Ru$ [M-3H]$^-$: 1884.34), *m/z* 1750.9 (-CpAp) (calcd mass for $C_{57}H_{66}N_{21}O_{30}P_4Ru$ [M-(*p*-cym)-3H]$^-$: 1750.23), *m/z* 1727.0 (-CpAp) (calcd mass for $C_{59}H_{74}N_{17}O_{30}P_4Ru$ [M-bpm-3H]$^-$: 1726.28), *m/z* 1492.9 (-CpAp) (calcd mass for $C_{49}H_{62}N_{17}O_{30}P_4$ [M-(*p*-cym)-Ru-bpm-H]$^-$: 1492.29), *m/z* 1188.3 (-CpApTp) (calcd mass for $C_{39}H_{49}N_{15}O_{23}P_3$ [M-(*p*-cym)-Ru-bpm-H]$^-$: 1188.23).

D.3) Adduct $^{5'}$*dCAT**GG**CT-[Ru(bpm)]*$^{2+}$ ***6c***: R_t= 18.6 min (gradient: 5 to 45% in 30 min). HR ESI-MS, negative mode: *m/z* 783.4331 (calcd mass for $C_{76}H_{88}N_{29}O_{41}P_6Ru$ [M-5H]$^{5-}$: 783.4387), *m/z* 587.3270 (calcd mass for $C_{76}H_{87}N_{29}O_{41}P_6Ru$ [M-6H]$^{4-}$: 587.3271). MALDI-TOF-MS, negative mode: *m/z* 2352.8 (calcd mass for $C_{76}H_{90}N_{29}O_{41}P_6Ru$ [M-3H]$^-$: 2352.33). MALDI-TOF-MS after digestion with snake venom phosphodiesterase: *m/z* 1759.9 (-pCpT) (calcd mass for $C_{57}H_{65}N_{24}O_{28}P_4Ru$ [M-3H]$^-$: 1759.24), *m/z* 1501.9 (-pCpT) (calcd mass for $C_{49}H_{61}N_{20}O_{28}P_4$ [M-Ru-bpm-H]$^-$: 1501.29). MALDI-TOF-MS after digestion with bovine spleen phosphodiesterase: *m/z* 1750.8 (-CpAp) (calcd mass for $C_{57}H_{66}N_{21}O_{30}P_4Ru$ [M-3H]$^-$: 1750.23), *m/z* 1492.8 (-CpAp) (calcd mass for $C_{49}H_{62}N_{17}O_{30}P_4$ [M-Ru-bpm-H]$^-$: 1492.29), *m/z* 1188.3 (-CpApTp) (calcd mass for $C_{39}H_{49}N_{15}O_{23}P_3$ [M-(*p*-cym)-Ru-bpm-H]$^-$: 1188.23). MALDI-TOF-MS after digestion with Nuclease S1: *m/z* 1222.1 (-$^{5'}$CpApTp, -$^{3'}$T) (calcd mass for $C_{37}H_{41}N_{17}O_{19}P_3Ru$ [M-3H]$^-$: 1222.10), *m/z* 1526.1 (-$^{5'}$CpAp, -$^{3'}$T) (calcd mass for $C_{47}H_{54}N_{19}O_{26}P_4Ru$ [M-3H]$^-$: 1526.15).

AUTHOR INFORMATION

Corresponding Authors

vmarchan@ub.edu
P.J.Sadler@warwick.ac.uk

ACKNOWLEDGMENT

This work was supported by funding from the Ministerio de Educación y Ciencia (CTQ2005-01834, CTQ2007-68014, CTQ2008-02064 and CTQ2010-21567), the Generalitat de Catalunya (2009SGR208 and Xarxa de Referència de Biotecnologia) and the Programa d'Intensificació de la Recerca (UB). L.S. was supported by a Marie Curie Intra European Fellowship 220281 (PHOTORUACD) within the 7th European Community Framework Programme and by ERC BIOINCMED (grant no 247450 to PJS). The authors acknowledge the use of the facilities of the Servei d'Espectrometria de Masses of the Universitat de Barcelona and provided by Science City (ERDF/AWM), and Dr. Lijiang Song at the University of Warwick for MS support.

ASSOCIATED CONTENT

Supporting Information. Details of the syntheses and characterization of the pyridyl-derivatized peptides **4** and **5**. Photoactivation experiments with conjugate **3**. Full characterization of adducts **7a-c** and **8a-c** and selected MS and UV-vis spectra and HPLC traces. This material is available free of charge via the Internet at http://pubs.acs.org.

ABBREVIATIONS

ACN, acetonitrile; bpm, 2,2'-bipyrimidine; cym, cymene (1-methyl-4-(1-methylethyl)benzene); DCM, dichloromethane; DIPC, *N,N'*-diisopropylcarbodiimide; DIPEA, *N,N*-diisopropylethylamine; DMF, *N,N*-dimethylformamide; DsaC, diaminosuberic acid *C*-terminus; Dsa*N*, diaminosuberic acid *N*-terminus; ESI, electrospray ionization; EtG, ethylguanine; Fmoc, 9-fluorenylmethyloxycarbonyl; HATU, (2-(7-Aza-1H-benzotriazole-1-yl)-1,1,3,3-tetramethyluronium hexafluorophosphate; HOAt, 1-hydroxy-7-azabenzotriazole; HOBt, 1-hydroxybenzotriazole; HR, high resolution; MALDI-TOF, matrix-assisted laser desorption ionization time-of-flight; py: pyridine; TIS, triisopropylsilane; TFA, trifluoroacetic acid.

REFERENCES

(1) Wheate, N. J.; Walker, S.; Craig, G. E.; Oun, R. *Dalton Trans.* **2010**, *39*, 8113-8127.

(2) (a) Jakupec, M. A.; Galanski, M.; Arion, V. B.; Hartinger, C. G.; Keppler, B. K. *Dalton Trans.* **2008**, 183-194. (b) Okarvi, S. M. *Cancer Treat. Rev.* **2008**, *34*, 13-26. (c) Moucheron, C. *New. J. Chem.* **2009**, *33*, 235-245. (d) Van Rijt, S. H.; Sadler, P. J. *Drug Discov. Today* **2009**, *14*, 1089-1097.

(3) (a) Aronov, O.; Horowitz, A. T.; Gabizon, A. Gibson, D. *Bioconjugate Chem.* **2003**, *14*, 563-574. (b) Brunner, J.; Barton, J. K., *Biochemistry* **2006**, *45*, 12295-12302. (c) Mukhopadhyay, S.; Barnes, C. M.; Haskel, A.; Short, S. M.; Barnes, K. R.; Lippard, S. J. *Bioconjugate Chem.* **2008**, *19*, 39-49. (d) Dhar, S.; Liu, Z.; Thomale, J.; Dai, H.; Lippard, S. J. *J. Am. Chem. Soc.* **2008**, *130*, 11467-11476. (e) Barragán, F.; Moreno, V.; Marchán, V. *Chem. Commun.* **2009**, 4705-4707. (f) de Jong, M.; Breeman, W. A. P.; Kwekkeboom, D. J.; Valkema, R.; Krenning, E. P. *Acc. Chem. Res.* **2009**, *42*, 873-880. (g) Puckett, C. A.; Barton, J. K. *Bioorg. Med. Chem.*, **2010**, *18*, 3564-3659. (h) Splith, K.; Hu, W.; Schatzschneider, U.; Gust, R.; Ott, I.; Onambele, L. A.; Prokop, A.; Neundorf, I. *Bioconjugate Chem.* **2010**, *21*, 1288-1296. (i) van Rijt, S. H.; Kostrhunova, H.; Brabec, V.; Sadler, P. J. *Bioconjugate Chem.* **2011**, *22*, 218-226. (j) Dhar, S.; Kolishetti, N.; Lippard, S. J.; Farokhzad, O. M. *Proc. Natl. Acad. Sci. USA* **2011**, *108*, 1850-1855.

(4) (a) Crespy, D.; Landfester, K.; Schubert, U. S.; Schiller, A. *Chem. Commun.* **2010**, *46*, 6651-6662. (b) Schatzschneider, U. *Eur. J. Inorg. Chem.* **2010**, 1451-1467. (c) Farrer, N. J.; Salassa, L. Sadler, P. J. *Dalton Trans.* **2009**, 10690-10701. (d) Farrer, N. J.; Sadler, P. J. *Aus. J. Chem.* **2008**, *61*, 669-674.

(5) (a) Mackay, F. S.; Woods, J. A.; Heringová, P.; Kaspárková, J.; Pizarro, A. M.; Moggach, S. A.; Parsons, S.; Brabec, V.; Sadler, P. J. *Proc. Natl. Acad. Sci. USA* **2007**, *104*, 20743-20748. (b) Phillips, H. I. A.; Ronconi, L.; Sadler, P. J. *Chem. Eur. J.* **2009**, *15*, 1588-1596. (c) Farrer, N. J.; Woods, J. A.; Salassa, L.; Zhao, Y.; Robinson, K. S.; Clarkson, G.; Mackay, F. S.; Sadler, P. J. *Angew. Chem. Int. Ed.* **2010**, *49*, 8905-8908.

(6) Betanzos-Lara, S.; Salassa, L.; Habtemariam, A.; Sadler, P. J. *Chem. Commun.* **2009**, 6622-6624.

(7) Pizarro, A. M.; Habtemariam, A.; Sadler, P. J. *Top. Organomet. Chem.* **2010**, *32*, 21-56.

(8) (a) Peacock, A. F. A.; Sadler, P. J. *Chem. Asian J.* **2008**, *3*, 1890-1899. (b) Levina, A.; Mitra, A.; Lay, P. A. *Metallomics* **2009**, *1*, 458-470. (c) Casini, A.; Hartinger, C. G.; Nazarov, A.; Dyson, P. J. *Top. Organomet. Chem.* **2010**, *32*, 57-80. (d) Gasser, G.; Ott, I.; Metzler-Nolte, N. *J. Med. Chem.* **2011**, *54*, 3-25. (e) Süss-Fink, G. *Dalton Trans.* **2010**, *39*, 1673-1688.

(9) (a) Garanger, E.; Boturyn, D.; Dumy, P. *Anti-Cancer Agents Med. Chem.* **2007**, *7*, 552-558. (b) Auzzas, L.; Zanardi, F.; Battistini, L.; Burreddu, P.; Carta, P.; Rassu, G.; Curti, C.; Casiraghi, G. *Curr. Med. Chem*, **2010**, *17*, 1255-1299.

(10) (a) Bauer, W.; Briner, U.; Doepfner, W.; Haller, R.; Huguenin, R.; Marbach, P.; Petcher, T. J.; Pless, J. *Life Sci.* **1982**, *31*, 1133-1140. (b) Janecka, A.; Zubrzycka, M.; Janecki, T. *J. Pept. Res.* **2001**, *58*, 91-107. (c) Weckbecker, G.; Lewis, I.; Albert, R.; Schmid, H. A.; Hoyer, D.; Bruns, C. *Nat. Rev. Drug Discovery* **2003**, *2*, 999-1017.

(11) (a) Reubi, J. C. *Endocr. Rev.* **2003**, *24*, 389-427. (b) Zaccaro, L.; del Gatto, A.; Pedone, C.; Saviano, M. *Curr. Med. Chem.* **2009**, *16*, 780-795. (c) Mezo, G.; Manea, M. *Expert Opin. Drug. Deliv.* **2010**, *7*, 79-96.

(12) (a) Huang, C. M.; Wu, Y. T.; Chen, S. T. *Chem. Biol.* **2000**, *7*, 453-461. (b) Fichna, J.; Janecka, A. *Bioconjugate Chem.* **2003**, *14*, 3-17. (c) Sun, L.-C.; Coy, D. H. *Drugs Future* **2008**, *33*, 217-223. (d) Haberkorn, U.; Eisenhut, M.; Altmann, A.; Mier, W. *Curr. Med. Chem.* **2008**, *15*, 219-234. (e) Ferro-Flores, G.; Ramirez, F. M.; Melendez-Alafort, L.; Santos-Cuevas, C. L. *Mini-Rev. Med. Chem.* **2010**, *10*, 87-97.

(13) D'Addona, D.; Carotenuto, A.; Novellino, E.; Piccand, V.; Reubi, J. C.; Di Cianni, A.; Gori, F.; Papini, A. M.; Ginanneschi, M. *J. Med. Chem.* **2008**, *51*, 512-520.

(14) (a) Dirscherl, G.; König, B. *Eur. J. Org. Chem.* **2008**, 597-634. (b) Gross, A.; Metzler-Nolte, N. *J. Organomet. Chem.* **2009**, *694*, 1185-1188. (c) Peindy N'Dongo, H. W.; Ott, I.; Gust, R.; Schatzschneider, U. *J. Organomet. Chem.* **2009**, *694*, 823-827. (d) Metzler-Nolte, N. *Top. Organomet. Chem.* **2010**, *32*, 195-217.

(15) Marchán, V.; Moreno, V.; Pedroso, E.; Grandas, A. *Chem. Eur. J.* **2001**, *7*, 808-815.

(16) (a) Marchán, V.; Pedroso, E.; Grandas, A. *Chem. Eur. J.* **2004**, *10*, 5369-5375. (b) Algueró, B.; López de la Osa, J.; González, C.; Pedroso, E.; Marchán, V.; Grandas, A. *Angew. Chem. Int. Ed.* **2006**, *45*, 8194-8197.

(17) (a) Novakova, O.; Chen, H.; Vrana, O.; Rodger, A.; Sadler, P. J.; Brabec, V. *Biochemistry* **2003**, *42*, 11544-11554. (b) Liu, H.-K.; Wang, F.; Parkinson, J. A.; Bella, J.; Sadler, P. J. *Chem. Eur. J.* **2006**, *12*, 6151-6165.

(18) Gossens, C.; Tavernelli, I.; Rothlisberger, U. *J. Phys. Chem. A* **2009**, *113*, 11888-11897.

(19) (a) Berners-Price, S. J.; Barnham, K. J.; Frey, U.; Sadler, P. J. *Chem. Eur. J.* **1996**, *2*, 1283-1291. (b) Reeder, F.; Guo, Z.; Murdoch, P. del S.; Corazza, A.; Hambley, T. W.; Berners-Price, S. J.; Chottard, J.-C.; Sadler, P. J. *Eur. J. Biochem.* **1997**, *249*, 370-382.

(20) Novakova, O.; Kaspárková, J.; Bursova, V.; Hofr, C.; Vojtiskova, M.; Chen, H.; Sadler, P. J.; Brabec, V. *Chem. Biol.* **2005**, *12*, 121-129.

(21) (a) Dorcier, A.; Dyson, P. J.; Gossens, C.; Rothlisberger, U.; Scopelliti, R., Tavernelli, I. *Organomet.* **2005**, *24*, 2114-2123. (b) Egger, A. E.; Hartinger, C. G.; Renfrew, A. K.; Dyson, P. J. *J. Biol. Inorg. Chem.* **2010**, *15*, 919-927.

(22) Magennis, S. W.; Habtemariam, A.; Novakova, O.; Henry, J. B.; Meier, S. L.; Parsons, S.; Oswald, I. D. H.; Brabec, V.; Sadler, P. J. *Inorg. Chem.* **2007**, *46*, 5059-5068.

(23) Marchán, V.; Rodríguez-Tanty, C.; Estrada, M.; Pedroso, E.; Grandas, A. *Eur. J. Org. Chem.* **2000**, 2495-2500.

Table of Contents artwork